Reactive Plasma Deposited Si-N Films for MOS-LSI Passivation

A. K. Sinha,* H. J. Levinstein, T. E. Smith, G. Quintana, and S. E. Haszko

Bell Laboratories, Murray Hill, New Jersey 07974

ABSTRACT

Amorphous Si-N films have been synthesized from SiH_4 and NH_3 by reactive plasma deposition at 275°C in an improved radial flow reactor. With appropriate control of machine and process variables, films have been made with Si/N ratio of 0.75-1.5, density of 2.8-2.2g cm^{-3}, refractive index of 1.9-2.3, stress of 2×10^9 dynes cm^{-2} compressive to 5×10^9 dynes cm^{-2} tensile, and electrical resistivity at 2×10^6 V/cm of 10^{20}-10^4 Ω-cm. The process is MOS compatible and it produces relatively thick (1 μm) crack-resistant Si-N films (at 450°-500°C) having excellent step coverage and good adhesion to both Au and Al metallization. This paper describes the deposition technique, effect of deposition parameters on various film properties, and the advantages these films offer in silicon integrated circuit technology.

In MOS-LSI technology, it is recognized that the effectiveness of the final passivation layer will, to a large extent, determine the ultimate reliability of the packaged device. The passivation layer is intended to protect sensitive areas of the device from outside contamination by, *e.g.*, Na^+ and moisture, and also to provide scratch protection for the Al metallization.

A potentially attractive material for this purpose is silicon nitride which provides an inert barrier (1, 2) to Na and H_2O as opposed to phosphosilicate glass (3) which acts as a "getter" for Na as well as moisture. However, the use of Si_3N_4 has been restricted because of the high temperatures ($\gtrsim$700°C) required for chemical vapor deposition of Si_3N_4 films (4) and because of high tensile stresses which limit the usable film thickness to ~2000Å (5).

Several investigations have been made concerning deposition of silicon nitride films at lower temperatures (<450°C) using an rf plasma to provide some of the activation energy needed for the reaction between SiH_4 and NH_3 or N_2 (6-10). The earlier systems utilized a quartz tube, an inductively coupled plasma, and gases flowing at a pressure of ~100 mTorr. These techniques generally lead to poor uniformity from wafer to wafer and inadequate step coverage. Reinberg (11) developed a radial flow reactor for Si-N deposition. He utilized a capacitively coupled rf discharge in a gas mixture consisting of SiH_4, NH_3, N_2, and Ar at relatively high pressures (0.5-1 Torr) and low powers (~50 W), in order to achieve good thickness uniformity and good step coverage. Rosler *et al.* (12) recently described a CVD process which also utilizes a radially symmetrical gas flow but in a direction opposite to that used by Reinberg; the capacitive discharge operates at a higher power (500W) and a relatively low frequency (50 kHz). Detailed data on the resulting $Si_xN_yH_z$ film composition ($0.8 \leq y/x \leq 1.0$), density (2.5-2.8 g cm^{-3}), resistivity (10^{15} Ω-cm), stress (1×10^9 dynes cm^{-2} compressive) etc., were reported by Kern and Rosler (13) for films deposited at 300°C.

We have devised certain improvements in the Reinberg radial flow reactor design which allows use of a wider range of deposition conditions and, consequently, a high degree of flexibility in tailoring the film properties (14). The main improvement consisted of a gas-flow discharge limiting shield which confines the plasma to a region above the substrates. It thereby enables use of higher rf powers without the adverse effects of a premature reaction between SiH_4 and NH_3 underneath the substrate table. This paper describes the deposition technique, effect of deposition parameters on various film properties, and the advantages these films offer in silicon integrated circuit technology.

Deposition Technique

Apparatus.—Figure 1 schematically shows the deposition apparatus consisting of a reactor, associated pumping systems, gas lines, and an rf power source.

The deposition reactor was a metal bell jar with a nominal diameter of 18 in. The cathode (16 in. diam) and the substrate table were made of Al and separated from each other by about 1 in. Heating was accomplished by means of quartz lamps mounted underneath the substrate table. A glow-discharge limiting shield was provided concentric with the heater and separated from it by ~¼ in. The gases were admitted underneath the heater, directed by the shield to flow radially inward over the surface of the substrate table and then exit to the pump through the center of the substrate table/heater assembly. Use of the gas flow discharge limiting shield eliminated premature decomposition of silane at higher rf powers since the gases were not exposed to the plasma until they were flowing over the substrates.

The pumping system was compatible with a high gas flow (>2 liters/min) at 1 Torr pressure. It consisted of a 150 cfm Leybold-Hereaus roots blower backed by two 17 cfm mechanical pumps running in parallel. The gas pressure was controlled by a throttle valve located in the roots blower line. The pressure was monitored

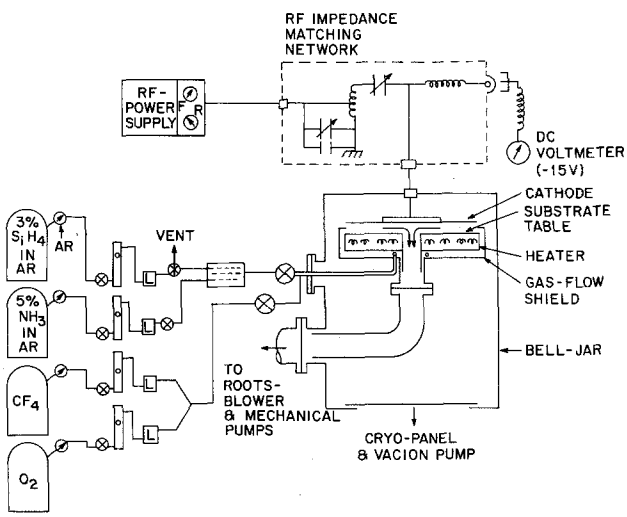

Fig. 1. Schematic of the apparatus used for deposition of RPD Si-N films.

* Electrochemical Society Active Member.

Key words: plasma-enhanced CVD, silicon nitride, thin films.

using a capacitance manometer (MKS Baratron) which provides measurements independent of the nature of the gas (and its conductivity). Facility was also provided to pump the system initially down to a base pressure of $\lesssim 10^{-6}$ mm with a cryopanel and a 400 liters/sec sputter-ion pump.

The reacting gases were 3% SiH_4 in Ar and 5% NH_3 in Ar. The delivery pressure was kept at 15 psig. The gases were led through rotameters to leak valves, L, and then on to a mixing chamber and finally to the deposition system. Special care was taken to keep these lines leak-tight. Similar but separate lines were provided for CF_4 and O_2 and an appropriate mixture of these two gases was used for plasma-etch cleaning of the station.

The rf power to the cathode was supplied by a Varian (13.56 MHz) power supply and an impedance-matching network of the conventional L-C type to which was added a fixed capacitor (Jennings, 220 pF) in parallel with the tunable load capacitor. This enabled satisfactory tuning with less than 10W reflected power at ~1 Torr pressure. The cathode d-c self-bias could be measured with a d-c voltmeter attached to the cathode power line via rf chokes.

Procedure.—The wafers (2 in. diam) were loaded in two concentric circles the bell jar was closed, and the system pumped down to $\sim 10^{-6}$ Torr using successively the mechanical pumps (to ~1 Torr), the roots blower (to ~3 mTorr), and the cryopanel and the sputter-ion pump (to $\sim 10^{-6}$ Torr). The final stage of the pumping added only 2-5 min to the total pumpdown time (~20 min). Next, the sputter-ion pump isolation valve was closed, the gases were admitted into the reactor, and the roots blower valve was opened again. A dynamic pressure (~600 mTorr) was established in the system with the gases flowing at the desired flow rates. Thereafter the roots blower valve was throttled to the desired pressure.

The rf plasma was excited to the desired power level. The plasma initiated and sustained the reaction between SiH_4 and NH_3 on the surface of the heated substrates. Typically, depositions were carried out for 1 hr to give Si-N films 1.1(±0.1) μm thick. The total turnaround time was <2 hr.

After every three runs, the system was cleaned *in situ* for 1-2 hr in a plasma (1000W) containing CF_4 + 8% O_2 at a flow of ~250 cm^3/min and a pressure of ~1000 mTorr with the substrate heater on. Subsequent to the cleaning operation a predeposition run (~15 min) was made with SiH_4 and NH_3 at the desired flows and pressure.

Film Evaluation Techniques

The film stress was deduced from change in curvature of the Si substrate due to the Si-N layer. For evaluation of 1 μm thick films, use was made of an optically levered laser beam to determine the substrate curvature (15). A more sensitive method was used for measurements on thinner films (~200Å); namely, the ABAC (automatic Bragg angle control) x-ray technique (16).

The refractive index was measured using an ellipsometer (5461Å). For film thickness and etch rate measurements, a step was etched in the film with 7:1 buffered HF (BHF) and the resulting step height was measured with the Talystep.

Rutherford backscattering analysis was used to determine the film composition and its density (17). Thinner films (~2000Å) on (111) Si were employed so as to get "clean" spectra and to reduce the background due to Si substrate by channeling along the [110] direction.

The density measured by Rutherford backscattering analysis was always within 10% and generally smaller than that determined from weight gain measurements on certain thicker films deposited under identical conditions (*e.g.*, conditions A and B of Table I).

The growth morphology of the film and its step coverage for various device topologies were determined using scanning electron microscopy on cleaved sections. The film structure was established using transmission electron microscopy in conjunction with selected area transmission electron diffraction.

The crack resistance of these films on various device structures was ascertained by heating them up to 450°-550°C (½ hr periods, air ambient), after which the films were examined in an optical microscope under interference contrast and/or polarized light. Usually when cracking occurred, it was gross and easily revealed. Further confirmation of the film integrity was provided by exposing the device structures to a metallization etch for 15 min followed by examination in the optical microscope.

Effect of Deposition Parameters

Five main process variables were investigated: (*i*) gas composition, (*ii*) total gas flow, (*iii*) pressure, (*iv*) substrate temperature, and (*v*) rf power to the plasma. Table I contains a summary of two "standard" processes (A and B) and the resulting film properties. Studies of variables (*i*) through (*iv*) were carried out in conjunction with process A, *i.e.*, at an rf power of 250W and with the remaining three parameters at the values given for process A.

Most of the data points, except those pertaining to "standard" processes A and B (Table I), represent averages of a limited number of measurements on 3-6 2 in. diam Si wafers located in the main outer row of the substrate table. In the worst cases, *i.e.*, at conditions farthest away from optimum, variations in some properties such as film thickness and etch rate could be as much as ±15%, but the uniformity improved to well within ±10% as the conditions approached optimum values.

Table I. Reactive plasma deposition conditions and resulting Si-N film properties for standard processes A and B

		Process A		Process B
A.	Reacting gases		$SiH_4/NH_3/Ar$	
B.	SiH_4 concentration (% flow)	1.70		1.78
	SiH_4/NH_3	0.71		0.79
C.	Total gas flow (sccm)		2320	
D.	Pressure (mTorr)		950	
E.	Substrate temperature (°C)		275	
F.	RF power (fwd/rev., W)	250/0		300/0
1.	Typical thickness (μm)		1.1 (±0.1)	
2.	Stress (10^9 dynes cm^{-2})	1-5, T		1, C
3.	BHF etch rate (Å/min)	100-200		75-150
4.	Refractive index	2.05 (±0.1)		1.95 (±0.1)
5.	Density (g cm^{-3})	2.55 (±0.05)		2.75 (±0.05)
6.	Composition (Si/N)	1.05 (±0.05)		0.8
7.	Cracking resistance (°C)	450		550
8.	Adhesion		Good	
9.	Step coverage		Excellent	
10.	Scratch resistance		Good	
11.	Dielectric constant	6.4		6.8
12.	Breakdown strength (10^6 V/cm)	3.9		5.0
13.	Resistivity at 2 × 10^6 V/cm (Ω-cm)	4 × 10^{13}		3 × 10^{15}

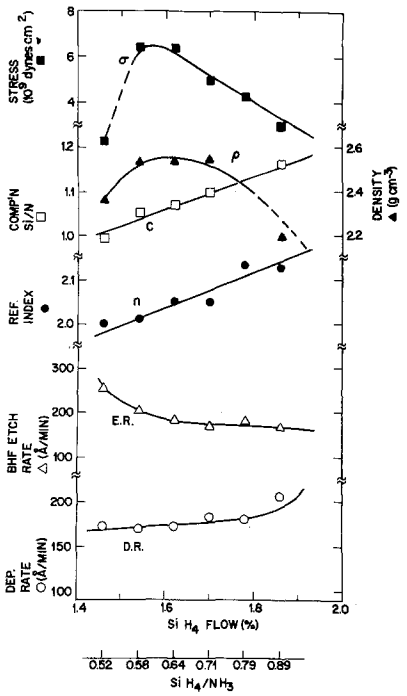

Fig. 2. Effect of SiH_4 concentration and SiH_4/NH_3 ratio on the properties of RPD Si-N films. (Other parameters kept constant at the values given for process A).

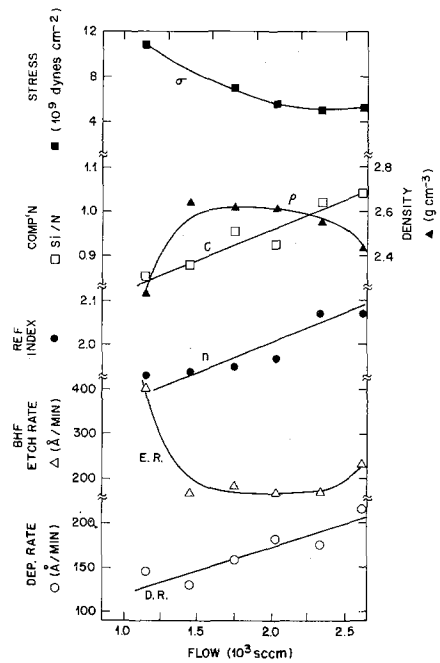

Fig. 3. Effect of gas flow on the properties of RPD Si-N films

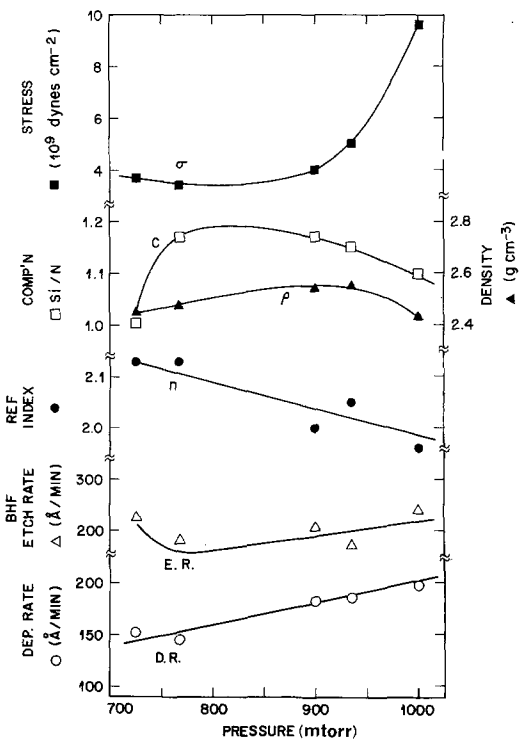

Fig. 4. Effect of gas pressure on the properties of RPD Si-N films

Gas composition.—Figure 2 shows the effect of increasing SiH_4 concentration ($1.4 \leq \%\ SiH_4 \leq 1.9$; $0.5 \leq SiH_4/NH_3 \leq 0.9$) on film properties for total flow of 2.3 std liters min^{-1}.

Increasing the SiH_4 concentration in the gas led to a corresponding linear increase in the Si/N ratio in the film (from ~1.0 to ~1.2) and a linear increase in the refractive index (from ~1.9 to ~2.2). With increasing SiH_4/NH_3 ratio, the film density ρ showed a broad peak ($\rho \approx 2.55$ g cm^{-3}) for $0.58 \leq SiH_4/NH_3 \leq 0.79$. The ρ decreased again at SiH_4/NH_3 ~0.9; however, this was not accompanied by a corresponding increase in the BHF etch rate, presumably because the films now had a much higher Si content (Si/N ~1.2). The film stress, σ, always tensile, showed a peak at SiH_4/NH_3 ~0.6, which is located at a slightly lower SiH_4 concentration than that for the peak in ρ. The choice of SiH_4/NH_3 ~0.7 for process A was selected on the basis of data on σ and ρ; one of the goals being to achieve a low σ in conjunction with high ρ (see section on Crack resistance, below).

Gas flow.—The total gas flow was varied in the range 1.0-2.5 liters min^{-1}, with the SiH_4/NH_3 ratio constant at 0.71 (Fig. 3) ($\%\ SiH_4 = 1.70$). Under these conditions, the Si/N ratio in the film varied from 0.8 to 1.05; for this composition range, the film density seems to have a dominant effect on the BHF etch rate; a broad maximum in ρ corresponds to a broad minimum in the etch rate. The tensile stress decreases with increasing flow; this is probably the result of a higher film purity (with respect to possible N_2 contamination, see below) as the flow is increased.

Pressure.—The total pressure during deposition was varied from ~700 to 1000 (±25) mTorr. As shown in Fig. 4, increasing the pressure led to a higher deposition rate, whereas the density or the BHF etch rate did not change much. The refractive index decreased linearly. This generally (*i.e.*, for pressures $\gtrsim$ 750 mTorr) correlates with a decrease in the Si/N ratio in the film. The stress remains nearly constant in the range 700-950 mTorr.

Substrate temperature.—The range of substrate temperatures studied was $200 \leq T_S \leq 300$°C (Fig. 5). Higher temperatures were not investigated because the nitride films were intended for use on Ti/Pd/Au as well as Al metallization. As shown in Fig. 5, T_S has a pronounced effect on the BHF etch rate, which decreases almost exponentially with increasing T_S. The decrease in BHF etch rate is associated with a linear increase in the film density, ρ, and in the refractive index, n. Thus, for films deposited at 200°C, the BHF etch rate was 700 Å/min, the density was ~2.3 g cm^{-3}, and the refractive index was ~1.85. Interestingly, these films also had a rather large Si/N ratio (~1.2) and a high tensile stress (7×10^9 dynes cm^{-2}). With increasing T_S, both σ and Si/N ratio in the film displayed a shallow minimum at ~250°C; however, a higher T_S of 275°C was preferred because it led to films with yet larger density (2.55 g cm^{-3}) and somewhat lower etch rate without an excessive increase in σ.

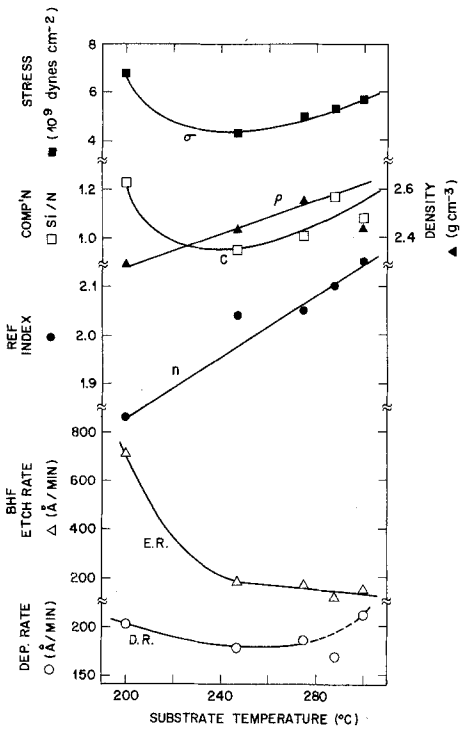

Fig. 5. Effect of substrate temperature on the properties of RPD Si-N films.

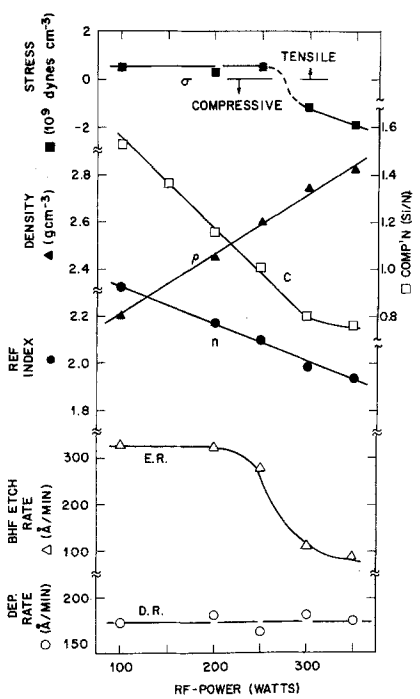

Fig. 6. Effect of rf power on the properties of RPD Si-N films. (Other parameters kept constant at values given for process B).

Rf power.—Tuned rf powers were investigated in the range 100-350W nominal, which were read off meters located at the power supply (Fig. 6). For this series of experiments, the SiH_4/NH_3 ratio was kept constant at 0.8 and % SiH_4 at 1.8. With increasing rf power, there is a rapid and linear increase in the film *P* (weight-gain measurements, using 1 μm thick films) from 2.2 g cm^{-3} at 100W to 2.8 g cm^{-3} at 350W. Films (1 μm) with Si/N >> 1 and lower density had a yellowish tinge when deposited on Al-metallized devices whereas those with Si/N $\lesssim$ 1 and densities $\gtrsim$ 2.4 g cm^{-3} appeared to be grayish and more transparent. Both the film σ and BHF etch rate showed a bimodal behavior at ~ 275W. Below this power level the stresses were very low tensile (~0.5 × 10^9 dynes cm^{-2}) and the etch rates were relatively high (275-325 Å/min). At rf powers $\gtrsim$ 300W, the stresses were compressive (1-2 × 10^9 dynes cm^{-2}) and the BHF etch rates were relatively low (~100 Å/min). Significantly, the refractive index decreased with increasing rf power, as did the Si/N ratio in the film. The latter, however, tended to level off at the stoichiometric value (Si/N ~ 0.75) for rf power > 300W.

The rf power readings quoted above are specific to the present system and its capacitive and inductive losses. It was found that the d-c (negative) voltage measured from cathode to ground was very small (1-10V). Peak-to-peak rf voltages were not measured, but since the cathode d-c voltages are small relative to gas ionization potentials [*e.g.*, 15.7 eV for Ar (18)], it is expected that the (positive) plasma potential with respect to ground must be quite high. This effect may be related to the system geometry, which consists of large electrodes (16 in. diam) in a relatively small volume (1 in. interelectrode spacing), and to the relatively large pressure (~ 1 Torr) of the discharge. These voltage characteristics may be contrasted with those present in typical rf sputtering systems (19), where the discharge operates at 5-10 mTorr pressure. The rf sputtering systems are associated with a very large cathode d-c self-bias of ~ 1 kV (19), which is nearly half the peak-to-peak or electron accelerating voltage. In such systems, the plasma is only slightly positive with respect to the ground.

Effect of N_2 and O_2 Additions to the Preferred Gas Mixture

Small amounts of air-leaks into the system, or substituting the NH_3 with N_2 as the source of N_2, were found to severely degrade the crack resistance. This was an unexpected observation since the literature contains examples of reactive plasma and reactive sputtering processes where preference is expressed for either N_2 (9) or NH_3 (6). Therefore, mixtures of NH_3 and N_2 were not suspect.

Figures 7 and 8 show the effect of N_2 addition on Si-N film properties. The control sample had a low tensile stress of 5 × 10^8 dynes cm^{-2}, an etch rate of 75 Å/min, and a refractive index of 1.92. Addition of small amounts of N_2 (up to 2%) caused a steep increase in tensile stress (up to 6 × 10^9 dynes cm^{-2}) as well as

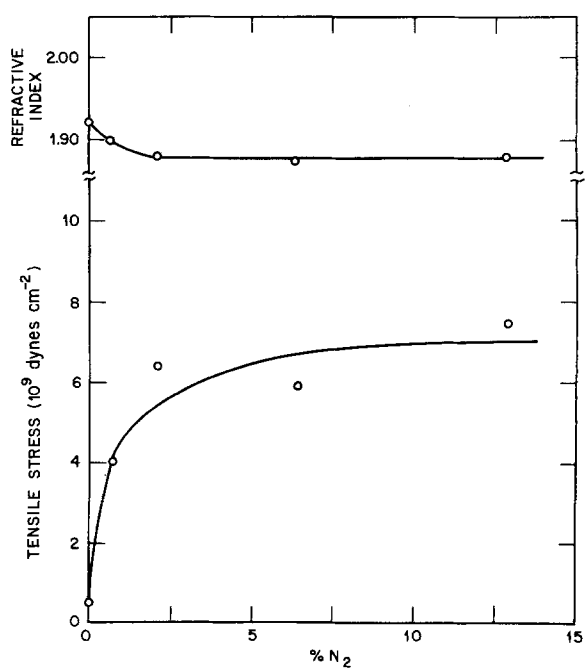

Fig. 7. Effect of N_2 additions to the reactant gas mixture (process A) on the tensile stress and refractive index of RPD Si-N films.

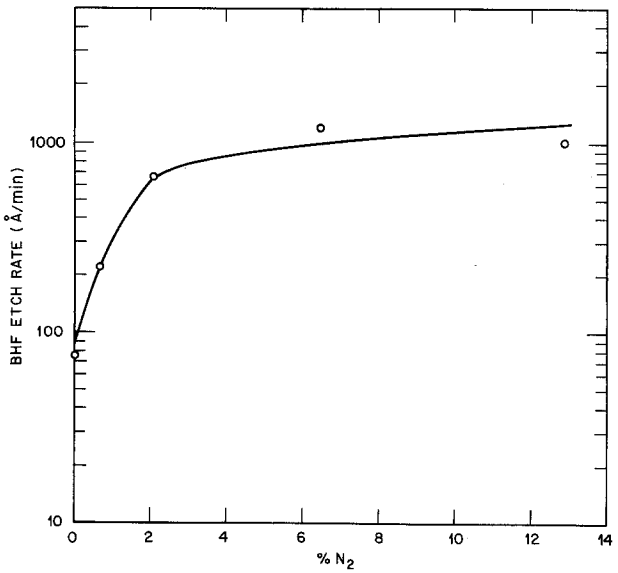

Fig. 8. Effect of N_2 addition to the reactant gas mixture on the etch rate in BHF of RPD Si-N films.

in the BHF etch rate (up to 700 Å/min) and a small decrease in the refractive index. At higher N_2 concentration in the gas stream, all of these film properties tend to level off. The high etch rate implies that these films have a lower density; the combination of low density and high tensile stress has been found to correlate with poor crack resistance of Si-N films at temperatures $\gtrsim$ 450°C (14, 15).

The addition of small amounts of O_2 to the reactant gas mixture had an even greater effect on BHF etch rate. As shown in Fig. 9, the etch rate continues to increase exponentially to ~3000 Å/min for 0.65% O_2, showing no sign of saturation. The effect on refractive index, n, is also quite severe (Fig. 10); n decreases from ~1.9 to ~1.6 for 0.65% O_2. The effect on film stress, σ, is relatively small. The σ initially increases to ~3 × 10^9 dynes cm^{-2} and then it decreases to almost zero for 0.65% O_2. It appears that some of the O_2 added to the gas stream gets incorporated into the film, leading to an oxynitride; hence the low n, very high etch rate, and the apparent stress-compensation effect (20).

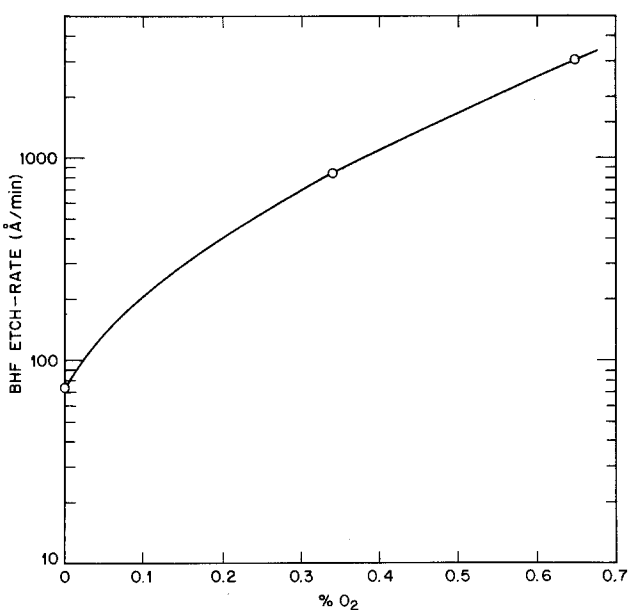

Fig. 9. Effect of O_2 addition to the reactant gas mixture on the BHF etch rate of RPD Si-N films.

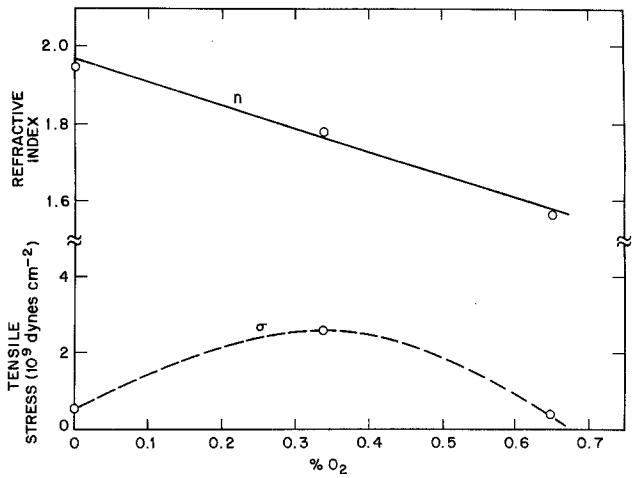

Fig. 10. Effect of O_2 addition to the reactant gas mixture on the tensile stress and refractive index of RPD Si-N films.

Discussion of Film Properties

Crack resistance.—Thick Si-N films (1 μm) on Al-metallized wafers cracked on heating to 450°C if the film stresses were too high ($\gtrsim$ 8 × 10^9 dynes cm^{-2}) or if the densities and deposition temperatures were too low ($\lesssim$ 2.2 g cm^{-3} and $<<$275°C, respectively). An example of extensive nitride cracking over both Al metallization and dielectric areas is shown in Fig. 11 for a Si-N film made at 250°C with a density of ~2.2 g cm^{-3} and a tensile stress of ~0.5 × 10^9 dynes cm^2. In contrast, films made using process A withstood 450°C, ½ hr treatments and those using process B did not show any cracking even at 550°C, ½ hr when the underlying Al was properly stabilized and it did not form large hillocks that punched through the Si-N film. Thermal stresses in Al, which form the driving force for hillock formation, have been shown to be a sensitive function of the film thickness and the initial microstructure (21). Most of our studies involved Al metallization (1-2 μm) evaporated at ~300°C and H_2 baked at 450°C prior to Si-N deposition.

It was recently proposed (14, 15) that the cracking resistance, CR, of a thick Si-N film at a given temperature T is functionally related to its density, ρ, intrinsic stress, σ_i, thermal mismatch, $\Delta\alpha$, with Si, and the deposition temperature, T_s, through the following equation (14)

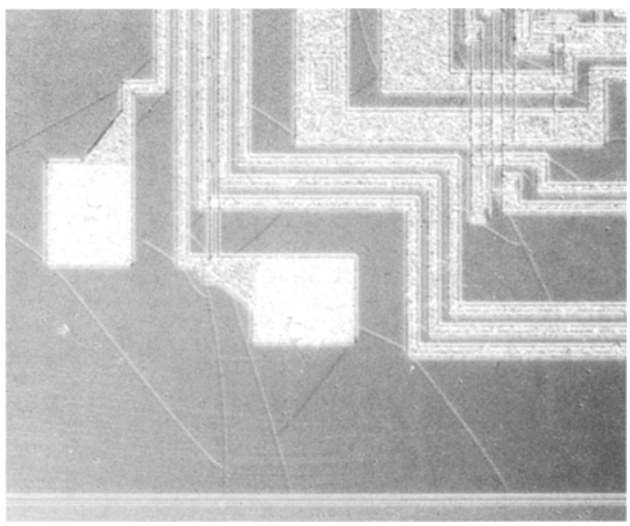

Fig. 11. Effect of a 450°C, ½ hr, air heat-treatment on the integrity of RPD Si-N film over Al-metallized Si wafer (film made at 250°C with a density of ~ 2.2 g cm^{-3} and a stress of ~ 0.5 × 10^9 dynes cm^{-2}).

$$CR \approx \frac{\rho}{\rho_o} \cdot \sigma_u - \sigma_i - \frac{E'}{1-\nu'} \int_{T_s}^{T} \Delta\alpha \cdot dT$$

Where, σ_u is the ultimate tensile stress of a structurally "perfect" Si_3N_4 film with density ρ_o, and E' and ν' are the Young's modules and Poisson's ratio for the film. This equation correctly predicts that CR will be improved if ρ is increased, σ_i and $\Delta\alpha$ are made small, and T_s is made high relative to the test temperature. A quantitative application of the above equation, including thermal stress measurements, for various Si-N films is described in Ref. (15).

Thickness uniformity.—The radial symmetry of gas flow and of plasma electron density inherent in the reactor design provides a useful means of attaining good thickness uniformity on wafers arranged in concentric circles. There still remains the problem of uniformity as a function of radius of the circle in which the wafers are placed. Here, two opposing effects may be involved (11): (*i*) the reactant gas concentration, which gets depleted as the gases flow inward; high gas flow will prevent such depletion, which is also countered by increased velocity as the gases approach the center of the substrate table, and (*ii*) the electron density which depends on the rf power and increases on going toward the center of the substrate table. Therefore, in principle, uniformity can be optimized by adjusting the gas flow for a particular rf power or vice versa.

For the preferred processes (A and B of Table I), we employed both a relatively high throughput of the reactants (2.3 liters/min) and a high rf power (250 or 300W); conditions which are compatible with a fair degree of uniformity. The uniformity was better than ±10% from wafer-to-wafer (arranged in two circles containing 14 and 8, 2 in. diam wafers, respectively) and from one deposition run to the other. The best thickness uniformity was observed at the lowest powers investigated (100W at $T_s = 275°C$), but these films were unacceptable because of a tendency toward cracking at 400°C. At the higher rf powers (≥ 350W), the thickness uniformity got much worse and ±10% uniformity could be achieved only over wafers in the outer circle.

Structure and growth morphology.—The amorphous nature of the present Si-N films was established by transmission electron microscopy. No contrast effects due to crystallites or voids could be seen in the bright- or dark-field mode, and electron diffraction patterns showed broad, diffuse halos characteristic of amorphous structure. Further insight into the nature of these films has been obtained by Lorentz-Lorenz correlation of the data on the film density, composition, and refractive index (17). The resulting magnitudes of electronic polarizabilities (α) suggest that the effective size of "Si" in plasma Si-N is quite high and probably corresponds to that of a Si-H complex. The α_{Si} increases with Si/N ratio indicating that Si-H complexes assume an increasing role in Si-rich Si-N films.

The growth morphology, as revealed by SEM examination, was always found to be smooth (layered) on the various surfaces investigated (Si, SiO_2, Al_2O_3, Si_3N_4, Al, Pd, Au) provided these surfaces were clean. However, in certain cases, we observed sporadic incidence of nodular growth, or hillocks; an extreme case is shown in Fig. 12(a). The device area in Fig. 12(b) shows nodules only in the dielectric areas, and with adequate cleaning, the situation corresponded to that of Fig. 12(c) where only a layered growth was observed.

We have correlated the occurrence of nodular growth with surface contamination (from baked-on residues of photoresist and intentionally introduced Sn and Pb at monolayer levels) and/or particulate matter. The presence of such contamination apparently triggers a vapor-liquid-solid growth (22) and/or gas

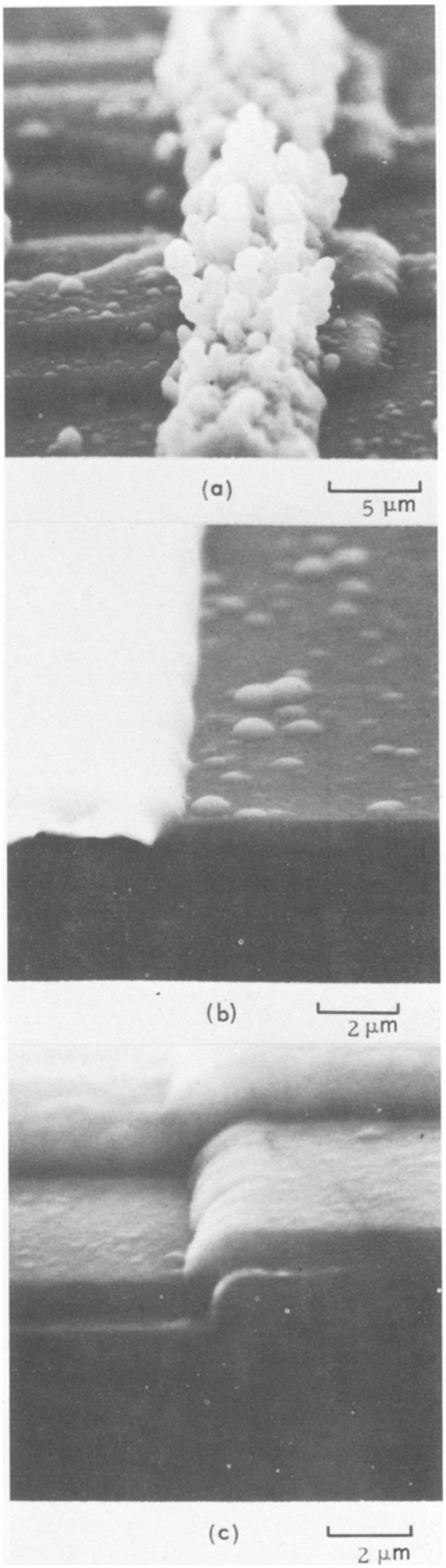

Fig. 12. Growth morphology of RPD Si-N films showing: (a) and (b) sporadic nodular growth (hillocks) on contaminated areas of device wafers, namely, Au lines and dielectric areas, respectively, and (c) layered growth on properly cleaned device wafers.

phase reaction (13) in the vicinity of the contaminated area. Such reactions in response to surface contamination were found to be more likely to occur under conditions of higher temperatures and larger flows, which also lead to "superior" crack-resistant films. Proper cleaning of the metallized wafers to remove any particulates and surface chemical contamination prior to H_2 bake was found to be desirable. One effective cleaning process involved scrubbing both sides of the wafer in Triton X (Rohm & Haas, Philadelphia, Pennsylvania) (1:20,000 dilution), followed by boiling in a mixture of 90% water and 10% H_2O_2 (high purity) for 10 min, followed by a cold deionized water rinse for $\geq$ 15 min.

Step coverage.—Use of high pressures (relative to sputtering) during deposition and a surface-activated film growth process leads to excellent step coverage as illustrated in Fig. 13 and 14 for Ti/Pd/Au beam leads and Al metallization, respectively. As shown in Fig. 14(c), the Si-N layer conforms well to the underlying topology even where the walls are vertical or they have a slight negative slope. Particularly important is the absence of any reentrant angles at the bottom of the steps. Further evidence of excellent step coverage was obtained by immersing the coated device wafers for $\geq$15 min in an appropriate metallization etch, such as hot H_3PO_4-CH_3COOH-H_2O for Al and KI-I_2 for Au, and then finding no attack on the underlying metal.

Si-gate MOS device compatibility.—MOS measurements were made on Si-gate MOS devices processed through second-level metallization and then subjected to the Si-N reactive plasma deposition, plasma etching of Si-N, and O_2 plasma stripping of the resist. The gate oxide capacitors showed no measurable increases in the oxide fixed charge or the surface-state density at midgap nor any radiation-induced bias-temperature instability. The absence of radiation-damage in above structures where the gate oxide is protected against soft radiation damage by the poly-Si appears to be due mainly to the use of relatively high pressures in the plasma and low levels of cathode d-c bias, as compared to rf or d-c sputtering processes.

Electrical properties of the present films were found to be a function of the film composition and its structures (23). The electrical resistivities (at 2×10^6 V/cm) for films with Si/N of 1.8, 1.0, and 0.75 were 4×10^4, 4×10^{13}, and 5×10^{19} Ω-cm, respectively. The dielectric strength similarly increased from 0.8 → 3.9 → 8.1 MV/cm. The thermal activation energy for conduction was ~0.3 eV. The dielectric constant (1 MHz) ranged from 6 to 8.

The Si-N films have been successfully utilized to form structures containing Ti/Pt/Au beam leads on Al (Fig. 15); the device is effectively sealed by the combination of Au-beam leads and plasma SiN. Si-gate PMOS and CMOS logic devices have been fabricated with the above structure in plastic packages; the latter devices showed an extrapolated median time to failure of > 40,000 hr under bias-humidity-temperature (85°C/85% RH) aging with intentional ionic contamination present. No cases were encountered of any cathodic corrosion of Al after 10^6 device-hours of 85/85 aging.

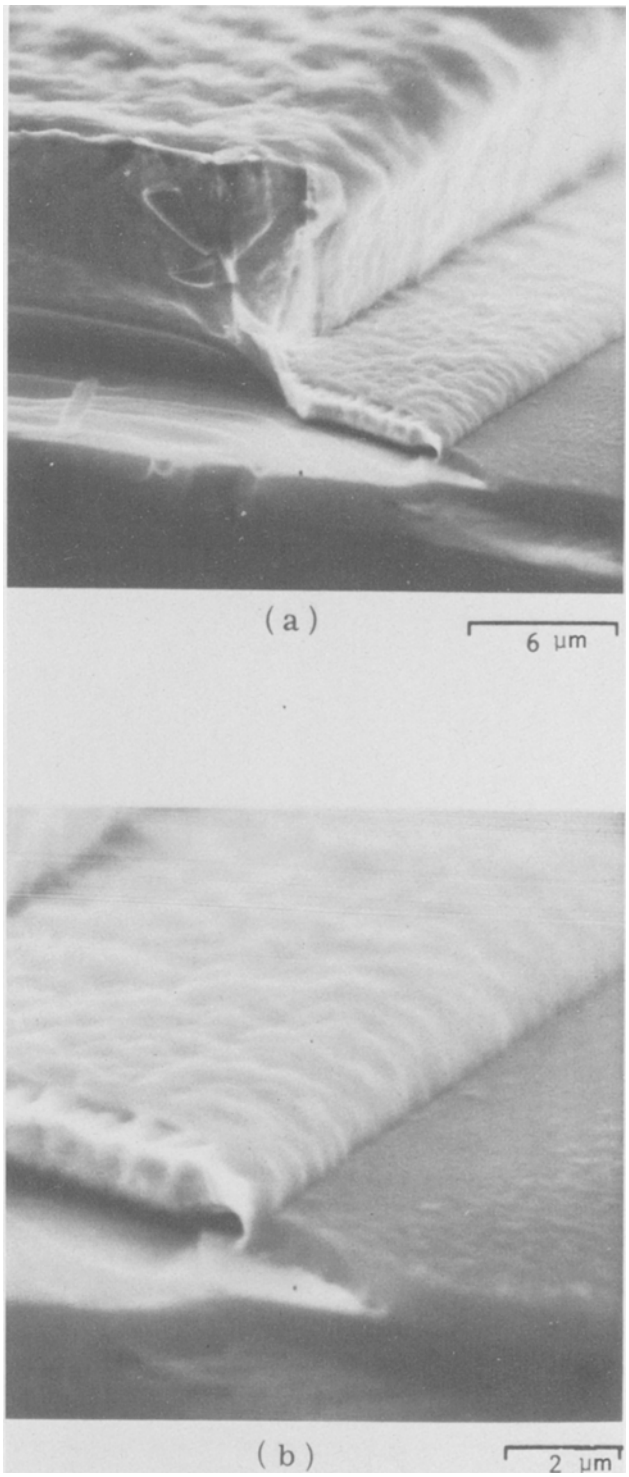

Fig. 13. SEM photographs of step coverage by 1 μm thick Si-N film on Au beams: (a) thick (12 μm) Au on Au (1 μm)/Pd/Ti metallization, (b) detail of base of the Au beam.

Conclusions

Certain plasma deposited Si-N films may compare favorably with PSG passivation layers and even with CVD Si_3N_4. Thus, these Si-N films provide an inert barrier to Na and H_2O, unlike heavily doped, low temperature CVD (LTCVD) P-glass which is hygroscopic and can react with H_2O to form corrosive H_3PO_4 (24). Si-N films have excellent step coverage whereas LTCVD often leads to films with a dog-bone type of feature on top and reentrant angles on the bottom of the steps. Si-N films provide a suitable surface for subsequent deposiiton of Ti/Pt/Au films whereas the surfaces of undensified P-glass are such that it is difficult to deposit adherent films on it. The electrical resistivity and the density of plasma Si_3N_4 films are comparable with those of CVD Si_3N_4, but the former can have much lower and compressive stresses which allows a higher usable thickness of 1 μm.

In conclusion, plasma-enhanced CVD provides an attractive deposition technique for Si-N films for final passivation. Its advantages are: manufacturability, low temperature operation, good step coverage/uniformity, compatibility with Si-gate MOS devices, and great flexibility with regard to control of stresses, film composition, density, and cracking resistance. The dis-

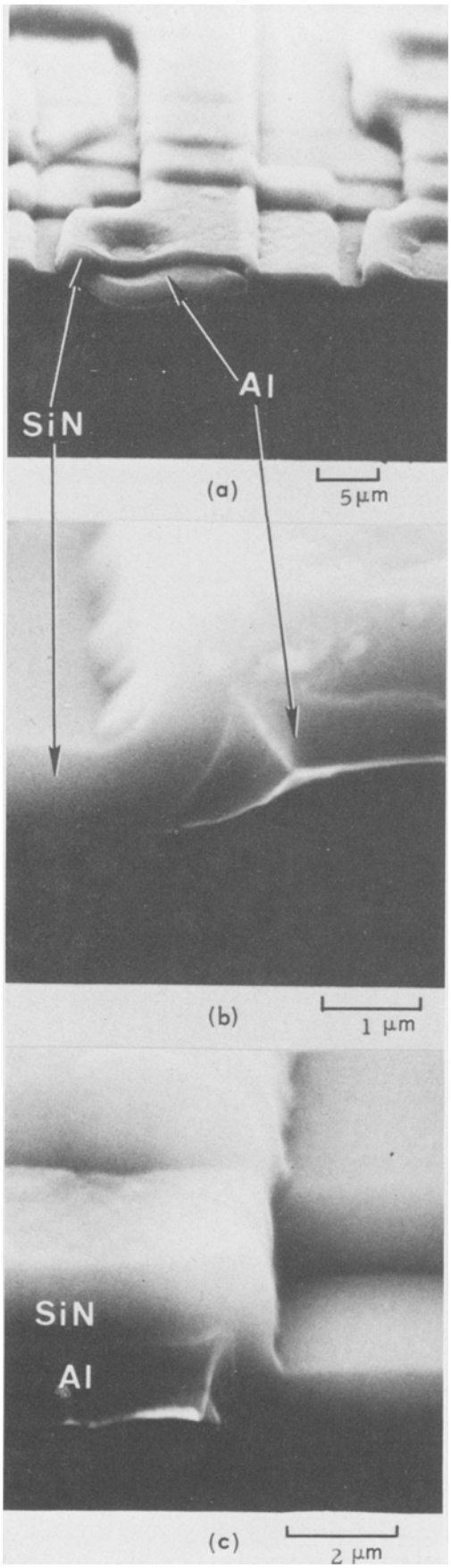

Fig. 14. Step coverage by RPD Si-N films on an Al-metallized LSI device: (a) section showing contact areas and Al runners, (b) detail of Si-N on Al with tapered edges, (c) Si-N on Al runner with nearly vertical edges.

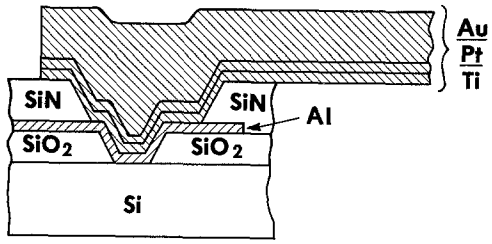

Fig. 15. Ti/Pt/Au beam leads to Al metallization passivated with RPD Si-N (Si/N = 1).

advantages are: a relatively complex reactor and process (many variables) and a sensitive growth morphology under certain conditions.

Acknowledgments

The authors would like to thank P. D. Cruzan and J. V. Dalton for experimental assistance, J. M. Dishman for MOS evaluations, J. M. Poate and E. Lugujjo for Rutherford backscattering analysis, T. T. Sheng for transmission electron microscopy, and R. S. Wagner for many useful discussions.

Manuscript submitted Oct. 19, 1977; revised manuscript received Dec. 1, 1977.

Any discussion of this paper will appear in a Discussion Section to be published in the December 1978 JOURNAL. All discussions for the December 1978 Discussion Section should be submitted by Aug. 1, 1978.

Publication costs of this article were assisted by Bell Laboratories.

REFERENCES

1. J. V. Dalton and J. Drobek, *This Journal*, **115**, 865 (1969).
2. M. T. Duffy and W. Kern, *RCA Rev.*, **31**, 742 (1970).
3. D. R. Kerr, J. S. Logan, P. J. Burkhardt, and W. A. Pliskin, *IBM J. Res. Dev.*, **8**, 376 (1964).
4. V. Y. Doo, D. R. Kerr, and D. R. Nichols, *This Journal*, **115**, 61 (1968).
5. W. A. Kohler, *Trans. AIME*, **246**, 735 (1970).
6. R. C. G. Swann, R. R. Mehta, and T. P. Cage, *This Journal*, **114**, 713 (1969).
7. H. F. Sterling and R. C. G. Swann, *Solid-State Electron.*, **8**, 653 (1965).
8. Y. Kuwano, *Jpn. J. Appl. Phys.*, **7**, 88 (1968).
9. R. Gereth and W. Scherber, *This Journal*, **119**, 1248 (1972).
10. O. Meyer and W. Scherber, *J. Phys. Chem. Solids*, **32**, 1909 (1971).
11. A. R. Reinberg, Abstract 6, p. 19, The Electrochemical Society Extended Abstracts, Spring Meeting, San Francisco, California, May 12-17, 1974; U. S. Pat. 3,757,733.
12. R. S. Rosler, W. C. Benzing, and J. Baldo, *Solid-State Technol.*, **19**, 45 (1976).
13. W. Kern and R. S. Rosler, *J. Vac. Sci. Technol.*, **14**, 1082 (1977).
14. A. K. Sinha, Abstracts 242, 244, pp. 625, 626, 629, 630, The Electrochemical Society Extended Abstracts, Fall Meeting, Las Vegas, Nevada, Oct. 17-22, 1976.
15. A. K. Sinha, H. J. Levinstein, and T. E. Smith, To be published in *J. Appl. Phys.*
16. G. A. Rozgonyi and T. Ciesielka, *Rev. Sci. Instrum.*, **44**, 1053 (1973).
17. A. K. Sinha and E. Lugujjo, *This Journal*, **123**, 189C (1976); *Appl. Phys. Lett.*, **32**, 245 (1978).
18. E. U. Condon and H. Odishaw, "Handbook of Physics," pp. 7-35, McGraw-Hill Book Co., New York (1967).
19. J. L. Vossen and J. J. O'Neill, *RCA Rev.*, **29**, 149 (1968).
20. C. M. Drum and M. J. Rand, *This Journal*, **115**, 194C (1968).
21. A. K. Sinha and T. T. Sheng, *Thin Solid Films*, **48**, 117 (1978).
22. R. S. Wagner and W. C. Ellis, *Trans. AIME*, **223**, 1053 (1965).
23. A. K. Sinha, *J. Electron. Mater.* **5**, 441 (1976); A. K. Sinha and T. E. Smith, To be published in *J. Appl. Phys.*
24. N. Nagasima, H. Suzuki, K. Tanaka, and S. Nishida, *This Journal*, **121**, 434 (1974).